# Agglomeration of *Escherichia coli* with positively charged nanoparticles can lead to artifacts in a standard *Caenorhabditis elegans* toxicity assay

Shannon K. Hanna [#*], Antonio Montoro Bustos, Alexander W. Peterson, Vytas Reipa, Leona D. Scanlan†, Sanem Hosbas Coskun, Tae Joon Cho, Monique E. Johnson, Vincent A. Hackley, Bryant C. Nelson, Michael R. Winchester, John T. Elliott, Elijah J. Petersen

Materials Measurement Laboratory, National Institute of Standards and Technology, 100 Bureau Drive, Gaithersburg, MD 20899-8313

[#] Current address: Center for Tobacco Products, Food and Drug Administration, 10903 New Hampshire Avenue, Silver Spring, MD 20993

† Current address: Department of Pesticide Regulation, California Environmental Protection Agency, 1001 I Street, Sacramento, CA 95814

* Corresponding author: hanna.shannonk@gmail.com

## Abstract

The increased use and incorporation of engineered nanoparticles (ENPs) in consumer products requires a robust assessment of their potential environmental implications. However, a lack of standardized methods for nanotoxicity testing has yielded results that are sometimes contradictory. Standard ecotoxicity assays may work appropriately for some ENPs with minimal modification, but produce artifactual results for others. Therefore, understanding the robustness of assays for a range of ENPs is critical. In this study, we evaluated the performance of a standard *Caenorhabditis elegans* (*C. elegans*) toxicity assay containing an *Escherichia coli* (*E. coli*) food supply with silicon, polystyrene, and gold ENPs with different charged coatings and sizes. Of all the ENPs tested, only those with a positively charged coating caused growth inhibition. However, the positively charged ENPs were observed to heteroagglomerate with *E. coli* cells, suggesting that the ENPs impacted the ability of nematodes to feed, leading to a false positive toxic effect on *C. elegans* growth and reproduction. When the ENPs were tested in two alternate *C. elegans* assays that did not contain *E. coli*, we found greatly reduced toxicity of ENPs. This study illustrates a key unexpected artifact that may occur during nanotoxicity assays.

## Introduction

An ever-increasing number of nano-enabled products and processes suggest that engineered nanoparticles (ENPs) may be released into various environmental matrices. This has spurred researchers to study the potential toxicological effects of ENPs on environmental and biological systems at an ever increasing pace and resulted in more than 10 000 papers published on nanotoxicology by 2013.[1] However, properly testing ENPs in relevant exposure scenarios using appropriate controls can be complicated due to the unique physiochemical nature of ENPs. This

has resulted in a request for robust, "standardized" assays that can be used to assess the potential ecological or human health impacts of ENPs.[2-6]

Evaluation of ecotoxicity test guidelines from the Organisation for Economic Co-operation and Development (OECD) for use with ENPs indicated that the majority of OECD test guidelines for toxicological testing are generally applicable for ENPs but adaptations may be needed because these tests were designed mainly for chemicals that readily dissolve in water.[6,7] One key challenge in using previously developed ecotoxicity tests with ENPs is that the ENPs may cause unexpected artifacts in nanoecotoxicity assays, such as the adsorption of key micronutrients in the test media, thus resulting in an indirect toxic effect. However, it is generally challenging to predict *a priori* which ENPs will cause artifacts because different ENPs may cause artifacts in various assays. To assess the robustness of a nanoecotoxicity assay, it is thus important to evaluate its performance across a range of ENPs that vary in size, surface chemistry, surface charge, and elemental composition spanning the broad array of properties for commercially produced ENPs. One approach to identify artifacts in toxicity assays that has been frequently used in algae and human cell viability nanotoxicity assays is the use of similar toxicity methods (e.g., assessing cell viability using both an assay based on metabolic activity and microscopic analysis).[8-10] In the absence of artifacts or biases, the results using similar methods should be comparable. However, this approach has rarely been applied to nanotoxicity assays involving multicellular organisms.

In this study, we examined the performance of an International Standardization Organization (ISO) *Caenorhabditis elegans* (*C. elegans*) assay (ISO 10872), a standardized method that has been widely used in the literature,[11-13] using silicon (Si), polystyrene (PS), and gold (Au) ENPs with a range of sizes (30 nm to 100 nm), surface coatings (polyvinylpyrrolidinone (PVP), polyethylene glycol (PEG), citrate (CIT), dendrimers, and branched polyethylenimine (bPEI)) and surface charges (positive, neutral, and negative). The Au ENPs were selected based on the commercial availability of nanoparticles with a range of surface coatings. The PS ENPs enabled comparisons to the results from our previous study[13] and the Si ENPs are a NIST reference material (RM) which enables other researchers to use these particles to directly compare their results to those obtained in this study. In the ISO assay, growth and reproduction are measured after a 4 d exposure during which *Escherichia coli* (*E. coli*) serves as a food source. To elucidate the extent to which potential interactions between ENPs and the *E. coli* food source in the ISO assay impacted the toxicity results, we also tested these particles using two assays that do not require a bacterial food source: a 6 d axenic toxicity assay with a fully defined medium[14] (Table S1) and a 24 h survival assay in M9.[15]

## Methods

### *ENP characteristics and preparation*

Most of the 30 nm, 60 nm, and 100 nm Au ENPs were purchased from nanoComposix (San Diego, CA), except for the 30 nm and 60 nm citrated coated particles which were NIST RMs as described

below. The characteristics of these commercial Au ENPs, as provided by the manufacturer, are given in Table S2. These Au ENPs had four different coatings: polyvinylpyrrolidinone (PVP), polyethylene glycol (PEG), citrate (CIT), and branched polyethylenimine (bPEI). Zeta potential (Z-P) and dynamic light scattering (DLS) measurements of the Au ENPs were obtained on the Zetasizer Nano (Malvern Instruments, Westborough, MA) as described in depth in the Supporting Information (SI). All of the Au ENPs were received suspended in deionized (DI) water. They were inverted several times before use to ensure homogeneity and then mixed with the relevant media to dilute them for dosing in the toxicity experiments as described in the "Toxicity assays" section below.

The citrate coated 30 nm National Institute of Standards and Technology (NIST) Reference Material (RM) 8012 Au ENP and 60 nm NIST RM 8013 Au ENP were purchased from NIST (Gaithersburg, MD) and have been used in studies on Au ENP uptake by *C. elegans*[16] and in mammalian cell cytotoxicity studies.[17] Dendron-encapsulated (PCD) Au ENPs were synthesized in house by the reduction of chloroauric acid in the presence of sodium borohydride and thioctic-tri-(PEG[600]-$NMe_3$).[18] The particles have a hydrodynamic diameter of 16.3 nm ± 0.5 nm (mean ± standard deviation) in DI water.[18]

The Si ENPs tested were modified from NIST RM 8027 (2 nm nominal diameter Si ENPs). Si ENPs were reconstituted into an aqueous solvent using hydrosilylation under UV-excitation.[19] Hydrosilylation allows for the exchange of the hydrophobic surface coating with positively (amine) charged moieties, rendering Si ENPs stably suspended in water. The reconstituted Si ENPs were dialyzed against DI water for three days with a 3 kD dialysis membrane prior to use. The pH was reduced from 10.6 to 7.2 using acetic acid. The concentration of the resulting suspension was measured via UV-VIS at an absorbance of 340 nm as described previously.[20] Polystyrene nanoparticles (PS ENPs) were purchased from Bangs Laboratories Inc. (Fishers, IN, USA). Characterization data for all ENPs tested is provided in Table S2.

*Toxicity assays*

*ISO 10872 Assay*. A detailed description of *C. elegans* culturing and the standard toxicity assay can be found in ISO 10872.[21] Wild type *C. elegans* nematodes and the OP50 strain of *E. coli* were purchased from the Caenorhabditis Genetics Center (CGC, University of Minnesota). *C. elegans* were maintained on nematode growth medium (NGM) with *E. coli* as feed. For the toxicity assay, eggs were obtained from gravid nematodes on mixed stage culture plates via bleaching. Briefly, to bleach mixed culture plates, 0.5 mL of 5 N NaOH and 1 mL bleach are added to a 10 mL conical centrifuge tube containing mixed stage nematodes and eggs. The tube was vortexed every 2 minutes for a total of 10 min. The tube was then centrifuged to pellet the eggs, the supernatant was removed, the egg pellet was rinsed with sterile water, vortexed, and the process was repeated twice more. Eggs were allowed to hatch overnight in DI water in a 20 °C incubator. An overnight culture of *E. coli* was pelleted and resuspended in M9 medium three times; M9 is a buffer containing 3.0 g $KH_2PO_4$, 6.0 g $Na_2HPO_4$, 0.5 g NaCl, 1.0 g $NH_4Cl$, in 1 L of DI water. The toxicity test was

conducted in 12-well plates, each well containing 10 juvenile nematodes, 500 µL of a 1000 formazin attenuation unit (FAU) suspension of *E. coli*, and 500 µL of the test solution/suspension. To prepare the test solution/suspension, ENPs or the reference chemical control were added to DI water at twice the desired concentration in 15 ml centrifuge tubes, mixed by inverting the tube, and added to the corresponding well containing 500 µL of the *E. coli* suspension. Benzylcetyldimethylammonium chloride (BAC-C16) was used as a reference chemical control and DI water was used as a negative control. Concentrations of ENPs in the ISO assay were ≈ 25 mg/L for all Au ENPs, 20 mg/L for Si ENPs, and 60 mg/L for PS ENPs. These concentrations were chosen as follows: the PS ENP concentration was chosen based upon results in our previous publication,[13] while the concentration for the other ENPs was based on the highest dose we could achieve using the ISO assay protocol for most of the ENPs: a 1:1 (volume: volume) dilution of the stock suspension concentration to yield a concentration of ≈ 25 mg/L. The selected BAC-C16 concentration was 15 mg/L based on the reported $EC_{50}$ reported in the ISO assay. After plating, the remaining juveniles not used in the assay were heated at 80 °C in an oven to kill and straighten the nematodes. The length of 30 nematodes was measured to obtain an average length. The test plates were placed in an incubator at 20 °C for 4 d (96 h) to allow for growth and reproduction. After 4 d, nematodes were heat killed at 80 °C. Entire wells were imaged under bright field microscopy using a CoolSNAPHQ2 CCD camera (Photometrics, Tucson, AZ) coupled to an automated Zeiss microscope (Axio Vert.A1, Carl Zeiss Microscopy, Oberkochen, Germany) with Zen software (Carl Zeiss Microscopy, 2012 Blue Edition). Images were stitched together in Zen. The length of adult hermaphrodites was measured and juveniles were counted using ImageJ (1.47v, Wayne Rasband, NIH, USA) to quantify growth and reproduction during the assay. More detailed information about the assay protocol, calculation of the percentage inhibition of growth or reproduction, and imaging procedure are provided in the SI and our previous publication.[13]

To further examine the interactions between Au ENPs and *E. coli*, enhanced darkfield microscopy was also employed. Au ENPs were mixed with an equal volume of M9 or *E. coli* (at 1000 FAU) in M9 and imaged using an enhanced dark-field condenser (CytoViva, Auburn, AL) attached to an Olympus BX-41 upright microscope with a 40X, 0.75 numerical aperture (NA) objective, 2X magnifier (total 80X magnification). This microscope system is capable of locating high scattering nanoscale objects such as metal nanoparticles.[22-24] A DAGE XL color CCD camera was used to collect images of the samples and understand the influence of media on particle agglomeration and to determine if *E. coli* cells and particles interact. To remove any organic residue and particulate matter prior to imaging, slides and cover slips were cleaned by bath sonication (20 min for each sonication step) in 1 % sodium dodecyl sulfate solution (v/v), rinsed with 18 MΩ cm DI water, bath sonicated in cold piranha solution (7:3 volume ratio of concentrated sulfuric acid and 30 % pure hydrogen peroxide), rinsed with 18 MΩ $cm^{-1}$ DI water, then sonicated, rinsed and stored in ethanol (100 % pure, The Warner-Graham Company, Cockeysville, MD). For imaging of only the Au ENPs, a 5 µL droplet of the stock suspension (concentrations of the stock suspensions are listed in Table S2) was added to the slide and a cover slip was immediately placed over the droplet. For imaging of Au ENP mixed with *E. coli*, the solutions were mixed in a microfuge tube for the

specific incubation time and then a 5 µL droplet was added to the slide/cover slip for imaging. A micrometer scale ruler was imaged under reflecting bright field conditions to calibrate the spatial dimensions of the CCD pixels. The CCD camera color response (color channel gain) was white balanced to the response of scattered white light from air dried NaCl crystals (acting as a 'white card' target for typical white balance adjustments), and these settings were fixed for the entire experiment. The CCD exposure time was set on a sample-by-sample basis from 1 ms to 300 ms to remain in a linear regime and not oversaturate the pixel values based upon the image histogram profile. Image analysis was performed using Fiji open source image analysis software.[25] The 24-bit color image was separated into a red, green, and blue image channel. An image that is the ratio value of red (R) to blue (B) was generated by dividing the red image channel by the blue image channel. The R/B ratio images for the homogeneous reference samples were used to create the appropriate threshold segmentation for particle size analysis and then applied to segmenting the R/B ratio values to distinguish between Au ENP / *E. coli* particle identity in heterogeneous samples.

*Axenic Assay*. For the axenic assay, nematodes were cultured as described by Samuel et al.[14] The toxicity assay was conducted in 12-well plates using time-synchronized eggs from bleached nematodes, similar to the ISO assay. However, for this assay, each well contained 350 µL of 2X modified *C. elegans* Habituation and Reproduction medium (mCeHR) (containing 400 µg/mL tetracycline-HCl, to avoid bacterial contamination), 150 µL of milk (Horizon Organic Fat Free Milk, Broomfield, Colorado, USA), and 500 µL of the test suspension. This mixture is similar to the recipe noted in Table S1, yet the medium prior to addition of the ENPs is double the concentration, tetracycline was added to avoid bacterial or fungal contamination, and milk was reduced from 20% of the total medium volume to 15% to allow for better imaging. Because only ten nematodes were present in each well, this reduction in milk did not impact growth and by the end of the assay, milk was still present in the medium by a colorimetric visual determination, indicating the nematodes did not consume it entirely. To prepare the test solution/suspension, ENPs or the reference chemical control were added to DI water at twice the desired concentration in 15 mL centrifuge tubes, mixed by inverting the tube, and 500 µL was added to the corresponding well containing 500 µL of mCeHR and milk mixture. BAC-C16 was used as a reference chemical control and DI water was used as a negative control for comparison with the other assays. All ENP concentrations were the same as the ISO assay except PS ENPs, which was increased to 200 mg/L, based on reduced toxicity of the BAC-C16. Additionally, the BAC-C16 concentration was increased to 50 mg/L to achieve a similar growth inhibition effect as the 15 mg/L used in the ISO assay. Ten juvenile nematodes were added to each well and the plates were placed in a 20 °C incubator for 6 d to allow for growth and reproduction. After 6 d, nematodes were heat killed at 80 °C, imaged, adult hermaphrodites were measured, and juveniles were counted with bright field imaging as described above. This assay required a longer incubation time than the ISO assay (6 d instead of 4 d) due to the slower growth of nematodes in axenic medium compared to those fed bacteria.[26]

*Acute Survival Assay*. The survival assay was conducted in 96-well plates containing L3 nematodes, 50 µL of M9 medium, and 50 µL of the test solution/suspension. BAC-C16 was also used as a chemical control. L3 nematodes were obtained by bleaching a mixed nematode plate, plating the eggs on an *E. coli* lawn, and allowing the plate to incubate at 20 °C for 24 h. Nematodes were then harvested by gently washing the plate with M9, being careful not to collect any *E. coli* in the nematode suspension. Five nematodes were added to each well of a 96-well plate containing the test suspensions. To prepare the test solution/suspension, ENPs or BAC-C16 were added to DI water at twice the desired concentration in 1.5 mL microcentrifuge tubes, mixed by inverting the tube, and added to the corresponding well containing 50 µL of M9. BAC-C16 was used as a reference chemical control and DI water was used as a negative control for comparison with the other assays. BAC-C16 concentration was decreased to 5 mg/L and 7.5 mg/L because all nematodes died after being exposed to a 15 mg/L concentration for 24 h. Plates were incubated at 20 °C for 24 h, at which point nematodes were scored as live or dead. Dead nematodes were normally straight but, if needed, nematodes were prodded to ensure mortality. All assays (ISO, axenic, and survival) were performed twice to confirm the reproducibility of the results.

*Statistical analysis*

Effects between groups for each *C. elegans* assay were compared (V 6.04, GraphPad Software, Inc.) using a Kruskal-Wallis test followed by Dunn's multiple comparisons test ($\alpha = 0.05$). For the ISO and axenic assays, at least six replicates were tested for each condition, while at least three replicates were tested for the survival assay. Statistical significance testing on the bacteria agglomerate sizes was performed on image analysis data (V 6.04, GraphPad Software, Inc.) using a one-way ANOVA test followed by Tukey's multiple comparison test after log transforming the data.

## Results and Discussion

Using the toxicity assay described in the ISO 10872 standard, the majority of ENPs tested had little to no impact on nematode growth or reproduction, suggesting low toxicity (Figure 1A and B). However, ENPs with positively charged coatings, such as bPEI (Au ENPs) or amine terminated (PS or Si ENPs), resulted in significant toxic effects in *C. elegans* ($p < 0.05$) as demonstrated by a greater than 50 % reduction in growth. Reproduction was also nonexistent for nematodes exposed to these positively charged (bPEI or amine) coated particles. In previous studies, surface charge has been implicated as one of the main factors influencing ENP toxicity with some studies suggesting that positively charged particles can be more toxic than negative or neutral particles,[27-31] while other researchers have found either no toxicity from positively charged Au ENPs[18] or that negatively charged ENPs were more toxic than neutral or positively charged particles.[32] In our previous study using the ISO 10872 assay and the positively charged polystyrene ENPs tested within this study,[13] feeding with dead bacteria instead of live bacteria resulted in a complete lack of growth inhibition of *C. elegans* up to a nanoparticle concentration of 60 mg/L, the concentration tested in this study. This suggests that the toxicity is not due to the positively charged ENPs

themselves but their interaction with the bacteria, which does not occur if the bacteria are dead. If any of the positively charged ENPs caused bacterial toxicity, this would be expected to decrease their toxicity to *C. elegans* as a result of decreased heteroagglomeration. Therefore, the toxicological effects to the *C. elegans* observed for the positively charged ENPs were not from bacterial toxicity.

Large agglomerates were visualized by microscopy in wells containing the positively charged ENPs after conducting the ISO assay (Figure 2), and there was a general trend of larger agglomerates with increasing ENP concentration (Figure S1). These agglomerates were not observed in the control wells or the wells after exposure to negative or neutral ENPs (Figure 2). Enhanced darkfield imaging was used to confirm and monitor the process of positively coated bPEI Au ENP agglomeration with *E. coli* over time. We observed agglomeration for bPEI coated Au ENPs incubated with *E. coli* (Figure 3A). Initial agglomeration appears as many small agglomerates ($\approx 10\ \mu m^2$) at early time points and then becomes fewer large size clusters ($> 100\ \mu m^2$) by the 24 h time point with few observable single (*i.e.*, non-agglomerated) Au ENPs or *E. coli*. In contrast, we observed no interaction or agglomeration for the neutral or negative coated Au ENPs as shown in the representative image for 30 nm PEG coated Au ENP and *E. coli* (Figure 3B and S2). Rather, the image shows primarily single Au ENPs (faint green) and *E. coli* (bright white). Image analysis was employed to segment the bacteria particle size and report the percentage of particles greater than $3\ \mu m^2$, the area larger than one single *E. coli* cell (Figure 3C). This shows that for all bPEI coated Au ENPs sizes (30 nm, 60 nm, and 100 nm), approximately 80 % of all *E. coli* had at least formed small-scale agglomerates by the 60 min exposure time. Analysis of average agglomerate size shows a gradually slower increase in the overall size of the bPEI – *E. coli* heteroagglomerates by the 24 h time point (Figure 3D). The average agglomerate size after 24 h appears to depend on the size of the bPEI coated Au ENPs with the 100 nm ENPs forming statistically larger agglomerates than the 30 nm or 60 nm ENPs (Figure 3D). In contrast, incubation of 30 nm PEG coated Au ENP with *E. coli* shows no increase in percent agglomeration or agglomerate size at any time point. The initial fast process of small agglomeration followed by a slow process of large cluster formation is consistent with previously described processes of particle heteroagglomeration.[33,34] In addition, the agglomerate sizes reported here were measured without solution agitation and were also in media without *C. elegans*.

We used color-based image analysis to confirm that the agglomerated clusters, shown in Figure 3A, consisted of both bPEI Au ENPs and *E. coli* particles (Figure 4). This color channel ratio analysis has been successfully employed before to detect protein binding to Au ENPs,[35] but it does not appear to have been used to characterize interactions between ENPs and cells. We imaged homogenous mixtures of all studied Au ENP coatings (PEG, PVP, CIT, and bPEI) and sizes (30 nm, 60 nm, and 100 nm) (Figure S2B). Subsequently, the red (R) channel of the color image was divided by the blue (B) channel to produce an image of R/B ratio values, and these R/B ratios were measured for each particle. The range of R/B ratios for each of the 30 nm, 60 nm, and 100 nm Au ENP sizes and *E. coli* bacteria were distinct (Figure 4B). Therefore, image thresholding using the

R/B ratios enabled identification of the particles and bacteria in images. The R/B ratios interpreted from Mie scattering theory[36] (Figure 4C) are in good agreement with those for Au ENPs measured here, except for CIT-Au ENPs (Figure 4D). All sizes of CIT-Au ENPs have similar R/B ratios to the 100 nm Au ENP size. Qualitatively, most Au particles in the CIT images appear similarly yellow-orange in color, but it is not clear why the CIT coating influences the particle color (data not shown). For both non-agglomerated and agglomerated heterogenous mixtures, the distinct R/B ratios for Au ENPs and *E. coli*, respectively, allow for image segmentation based upon particle identity (Figure 4E). Here, the 60 nm PEG coated Au ENPs with *E. coli* sample is used as a representative non-agglomerated mixture for neutral or negative coated Au ENPs where the particles are clearly visualized as being separate and non-interacting to demonstrate the efficacy of the R/B image segmentation procedure on this 'reference' sample. The analysis method is then applied to the 60 nm bPEI coated Au ENPs and *E. coli* sample after 24 h incubation, which is representative of a highly agglomerated mixture for positively charged ENPs. This analysis suggests the images of agglomerated clusters, in Fig 3A, are composed of 100 nm bPEI Au ENPs and *E. coli* according to their R/B ratios, when measured separately as homogeneous solutions. This behavior was also observed for the 60 nm bPEI Au ENPs (Figure 4E) and for the 30 nm bPEI Au ENPs (Figure 4B) but was not observed for the other Au ENPs (*e.g.*, 30 nm PEG Au ENPs Figure 3B). This data suggests that bPEI Au ENP do not form significant homoagglomerates while interacting with *E. coli*. For all other neutral or negative Au ENP particle coatings (PVP, PEG, CIT) at all studied sizes (30 nm, 60 nm, and 100 nm) no observable agglomeration or interactions were observed when exposed to *E. coli* (Figure 3B and S2).

The finding in our study that bPEI Au ENPs heteroagglomerate with *E. coli* cells is in accordance with a previous study that showed interactions with positively charged PEI and negatively charged *E. coli* cells.[37] Based upon the findings from this prior study, we hypothesize that the cells and polymer-coated Au ENPs flocculate via adsorption coagulation, which results in charge reversal and creates patchy surface charge, thus attracting more bPEI Au ENPs and more *E. coli* cells into the agglomerate. Other studies have reported flocculation of bacterial cells with positively charged ENPs that corresponded with toxicity.[38,39] However, some researchers refer only to the charge interaction that may cause physical damage or lead to ENPs entering the bacterial cells and report greater toxicity for positively charged ENPs compared to other ENPs.[30] *C. elegans* growth may have been inhibited in our study due to their inability to consume *E. coli* cells that were in these large agglomerates. *C. elegans* eat by pharyngeal pumping and normally consume *E. coli* cells that are approximately 2 µm in diameter. However, these agglomerates were much larger than 2 µm and we microscopically observed nematodes struggling to break off pieces of the agglomerates, suggesting that they were not able to feed properly (video S1). This decreased feeding is proposed as the mechanism that caused growth and reproduction inhibition.

To further evaluate this hypothesis, we examined the effect of ENPs on *C. elegans* in two assays without *E. coli*. In the axenic assay, none of the ENPs impacted growth of nematodes at the concentrations tested (25 mg/L for all Au ENPs and at 20 mg/L and 200 mg/L for the Si ENPs and

PS ENPs, respectively) except for the 2 nm Si ENPs (Figure 1C). Si ENPs inhibited growth by 29.0 % ± 13.5 % at 20 mg/L compared to the control (data reported for the axenic and ISO methods are mean ± standard deviation values; $n \leq 6$). However, other positively charged ENPs showed no impact on growth compared to the control. In fact, 50 mg/L BAC-C16 only reduced growth by 12.6 % ± 12.3 % in the axenic assay, compared to 15 mg/L of BAC-C16 inhibiting growth by 31.3 % ± 11.1 % in the ISO assay even though nematode length in the negative control groups was similar for both assays (ISO: 1437 µm ± 236 µm (n=140), axenic: 1305 µm ± 261 µm (n=90); data are mean ± 1 standard deviation value). Reproduction was highly variable compared to growth and, in many cases, ENP exposed nematodes had increased reproduction (exhibited in Figure 1D) compared to the control as indicated by the negative reproduction inhibition values. This result may stem from the worms utilizing the ENP coatings as a food source, a result previously observed for *Daphnia magna* exposed to lipid-coated carbon nanotubes.[40] Si ENPs were the only ENPs that significantly inhibited reproduction (Figure 1D). It is unclear if this effect is due to the very small size of the Si ENP (*e.g.* 2 nm). Agglomerates were also observed in the wells containing each of the positively charged ENPs, but they were much smaller than those observed in the ISO assay and did not appear to impact growth. The exact composition of the agglomerates is unknown due to the large number of components in the axenic media. Although our results show greatly reduced toxicity of BAC-C16 and no toxic impacts of any ENPs except for Si ENPs, multiple studies have demonstrated toxicity of dissolved organic and inorganic chemicals to *C. elegans* in axenic media,[41-43] thus indicating that an axenic assay is valuable for *C. elegans* toxicity testing.

We also examined toxicity via a short-term survival assay with only M9 and ENPs (no bacteria or nutrients) to avoid coating of the particles by constituents of the axenic media and heteroagglomeration of ENPs and bacteria. In these assays, we observed no toxicity for any ENPs after exposure for 24 h, but the nematodes were more sensitive to BAC-C16 than in the ISO assay even though both assays used M9 media (Figure 1E). At 5 mg/L of BAC-C16, only 68.9 % ± 14.3 % of nematodes survived, compared with little to no effect in the ISO assay at this concentration (data not shown), potentially due to the lack of food in the survival assay thereby making the nematodes more sensitive to the chemical. The lack of toxicity of any ENPs tested in this assay suggests that the interaction between the positively charged ENPs and *E. coli* exhibited in the ISO assay were the cause of the apparent toxicity of the positively charged ENPs. Several studies have used 24 h survival assays with *C. elegans* to assess toxicity of various substances [44,45], but this has been conducted less frequently with ENPs.[15] Similar to our findings for BAC-C16, *C. elegans* were more sensitive to Ag and Ag ENPs in a 24 h study in the absence of food [15] compared to a 72 h growth assay where a food source was present.[46] The sensitivity of nematodes in different life stages may have impacted our results as nematodes in the 24 h assay were L3 larva (hatched and molted twice) and those in the growth and reproduction assays were L1 (hatchlings) that later grew into adults. However, Donkin and Williams [47] tested various parameters in 24 h and 96 h survival assays with *C. elegans* and found that neither developmental stage nor the presence of *E. coli* impacted toxicity of ionic Cd, Pb, Cu, or Hg.

## Environmental Implications

While ENPs with positively charged amine or bPEI coatings reduced growth and reproduction of *C. elegans* in the ISO assay, toxicity assays in the absence of *E. coli* contradicted these results, except for the Si ENPs, and did not show a toxicological effect. Microscopic analysis revealed that interactions between positively charged ENPs and *E. coli* in the ISO assay created large heteroagglomerates. This may have led to a decrease in the availability of food which, in turn, inhibited the growth and reproduction of nematodes. Conducting nanoecotoxicity testing using axenic medium allowed us to avoid the interaction of ENPs with *E. coli*, resulting in no impact on *C. elegans* growth or reproduction for all of the ENPs except for the Si ENPs. However, results in axenic assays had higher variability compared to ISO assay results, especially for reproduction. Survival assays conducted in half-strength M9 with no food source over 24 h indicated no toxicity from any ENPs tested and an increased sensitivity to the reference chemical control, BAC- C16. The simplicity, lack of bacterial or media component interactions with ENPs, and sensitivity to the control detergent make the 24 h survival assay attractive as a potential standard ENP toxicity assay. In addition, the surface coating of ENPs can change in the environment as a result of either adsorption of natural organic matter which is ubiquitous in the natural environment or from adsorption of biomolecules after passage through organisms,[6,48] and thus the initial surface coating may not be the coating that organisms are exposed to in the natural environment.

The interaction between positively charged ENPs and *E. coli* in our study highlights the need to evaluate standardized toxicity assays for use with a broad range of ENPs. Unexpected ENP interactions during these assays may lead to test artifacts and false positives or negatives, similar to what we found in our study. In addition to assessing the robustness of the assay by testing a broad range of ENPs, there are additional approaches that can be taken to uncover potential artifacts in an ecotoxicity assay and improve its robustness for use with ENPs. Cause-and-effect analysis can be used to identify the impact of changes in an assay protocol, which are often needed when testing ENPs to accommodate the different behaviors of ENPs compared to dissolved chemicals, on its results and which assay steps contribute the most to the total variability.[49,50] Based on the results from cause-and-effect analysis, intermediate control measurements can be incorporated into the assay protocol to yield insights into the assay performance (e.g., how well were cells pipetted for cell-based assays) each time it is run and to monitor for changes in results of the assay process across time using control charting.[49-51] Interlaboratory testing can be critical for understanding the robustness of a protocol, because varying interpretations of a step in a protocol could lead to variable results and the ability to get harmonized results (e.g. within laboratory variability is equal to between laboratory variability) confirms that the assay can yield comparable results in different laboratories.[51-53] Given the substantial literature on potential artifacts in nanotoxicity assays, it is critical to conduct extensive control experiments to investigate if any artifacts observed in previous studies are encountered.[54,55] Building upon the results obtained in this study, other assays that rely upon feeding the organisms such as the *Daphnia magna* reproduction assay (OECD test 202) may also be impacted by heteroagglomeration between the

food source and the added ENPs. Lastly, conducting similar toxicological assays (e.g. evaluating cell viability using two different assays) to assess if comparable results are obtained can build confidence in the assay results if the assays operate on different principles since it is unlikely that they both would be impacted by the same biases.[51,56] Overall, robust, standardized toxicity assays will help ensure comparability between studies thereby supporting the successful application of nanoinformatics approaches, and decrease the potential for test result artifacts.


## Acknowledgements

NIST Disclaimer

Certain commercial products or equipment are described in this paper in order to specify adequately the experimental procedure. In no case does such identification imply recommendation or endorsement by the National Institute of Standards and Technology, nor does it imply that it is necessarily the best available for the purpose.

FDA Disclaimer

Although an author is currently an FDA/CTP employee, this work was not done as part of his official duties. This publication reflects the views of the authors and should not be construed to reflect the FDA/CTP's views or policies.


## Supporting Information

Supplemental methods describing zeta potential and dynamic light scattering measurements, axenic media, conduct of the ISO assay, imaging of the wells of the 12-well plates at the end of the assays, and calculation of growth and reproduction inhibition; figures showing increased heteroagglomeration of positively charged ENPs with higher ENP concentrations, and enhanced darkfield imaging of neutral or negatively charged Au ENPs; and tables showing the composition of the axenic assay media and physicochemical properties of the ENPs tested. This information is available free of charge via the Internet at http://pubs.acs.org.

## References


1. Krug, H. F., Nanosafety Research—Are We on the Right Track? *Angew. Chem. Int. Edit.* **2014,** *53* (46), 12304-12319.
2. Krug, H. F.; Wick, P., Nanotoxicology: An Interdisciplinary Challenge. *Angew. Chem. Int. Edit.* **2011,** *50* (6), 1260-1278.
3. Secondo, L. E.; Liu, N. J.; Lewinski, N. A., Methodological considerations when conducting in vitro, air–liquid interface exposures to engineered nanoparticle aerosols. *Crit. Rev. Toxicol.* **2017,** *47* (3), 225-262.
4. Rösslein, M.; Elliott, J. T.; Salit, M.; Petersen, E. J.; Hirsch, C.; Krug, H. F.; Wick, P., Use of cause-and-effect analysis to design a high-quality nanocytotoxicology assay. *Chem. Res. Toxicol.* **2015,** *28* (1), 21-30.
5. Piret, J.-P.; Bondarenko, O. M.; Boyles, M. S. P.; Himly, M.; Ribeiro, A. R.; Benetti, F.; Smal, C.; Lima, B.; Potthoff, A.; Simion, M.; Dumortier, E.; Leite, P. E. C.; Balottin, L. B.; Granjeiro, J. M.; Ivask, A.; Kahru, A.; Radauer-Preiml, I.; Tischler, U.; Duschl, A.; Saout, C.; Anguissola, S.; Haase, A.; Jacobs, A.; Nelissen, I.; Misra, S. K.; Toussaint, O., Pan-European inter-laboratory studies on a panel of in vitro cytotoxicity and pro-inflammation assays for nanoparticles. *Arch. Toxicol.* **2017,** *91* (6), 2315-2330.
6. Petersen, E. J.; Diamond, S. A.; Kennedy, A. J.; Goss, G. G.; Ho, K.; Lead, J.; Hanna, S. K.; Hartmann, N. B.; Hund-Rinke, K.; Mader, B.; Manier, N.; Pandard, P.; Salinas, E. R.; Sayre, P., Adapting OECD aquatic toxicity tests for use with manufactured nanomaterials: key issues and consensus recommendations. *Environ. Sci. Technol.* **2015,** *49* (16), 9532-9547.
7. Kühnel, D.; Nickel, C., The OECD expert meeting on ecotoxicology and environmental fate — Towards the development of improved OECD guidelines for the testing of nanomaterials. *Sci. Total Environ.* **2014,** *472*, 347-353.
8. Worle-Knirsch, J. M.; Pulskamp, K.; Krug, H. F., Oops they did it again! Carbon nanotubes hoax scientists in viability assays. *Nano Lett.* **2006,** *6* (6), 1261-8.
9. Hartmann, N. B.; Engelbrekt, C.; Zhang, J.; Ulstrup, J.; Kusk, K. O.; Baun, A., The challenges of testing metal and metal oxide nanoparticles in algal bioassays: titanium dioxide and gold nanoparticles as case studies. *Nanotoxicology* **2013,** *7* (6), 1082-1094.
10. Elliott, J. T.; Rösslein, M.; Song, N. W.; Blaza, T.; Kinsner-Ovaskainen, A.; Maniratanachote, R.; Salit, M. L.; Petersen, E. J.; Sequeira, F.; Lee, J.; Rossi, F.; Hirsch, C.; Krug, H. F.; Suchaoin, W.; Wick, P., Toward achieving harmonization in a nano-cytotoxicity assay measurement through an interlaboratory comparison study. *Altex* **2017,** *34* (2), 389-398.
11. Höss, S.; Frank-Fahle, B.; Lueders, T.; Traunspurger, W., Response of bacteria and meiofauna to iron oxide colloids in sediments of freshwater microcosms. *Environ. Toxicol. Chem.* **2015,** *34* (11), 2660-2669.
12. Angelstorf, J. S.; Ahlf, W.; von der Kammer, F.; Heise, S., Impact of particle size and light exposure on the effects of TiO2 nanoparticles on Caenorhabditis elegans. *Environ. Toxicol. Chem.* **2014,** *33* (10), 2288-96.
13. Hanna, S. K.; Cooksey, G. A.; Dong, S.; Nelson, B. C.; Mao, L.; Elliott, J. T.; Petersen, E. J., Feasibility of using a standardized Caenorhabditis elegans toxicity test to assess nanomaterial toxicity. *Environ. Sci. Nano* **2016,** *3*, 1080-1089.

14. Samuel, T. K.; Sinclair, J. W.; Pinter, K. L.; Hamza, I., Culturing Caenorhabditis elegans in Axenic liquid media and creation of transgenic worms by microparticle bombardment. *J. Vis. Exp.* **2014,** *(90)*, e51796.
15. Gorka, D. E.; Osterberg, J. S.; Gwin, C. A.; Colman, B. P.; Meyer, J. N.; Bernhardt, E. S.; Gunsch, C. K.; DiGulio, R. T.; Liu, J., Reducing environmental toxicity of silver nanoparticles through shape control. *Environ. Sci. Technol.* **2015,** *49* (16), 10093-8.
16. Johnson, M. E.; Hanna, S. K.; Montoro Bustos, A. R.; Sims, C. M.; Elliott, L. C. C.; Lingayat, A.; Johnston, A. C.; Nikoobakht, B.; Elliott, J. T.; Holbrook, R. D.; Scott, K. C. K.; Murphy, K. E.; Petersen, E. J.; Yu, L. L.; Nelson, B. C., Separation, sizing, and quantitation of engineered nanoparticles in an organism model using inductively coupled plasma mass spectrometry and image analysis. *ACS Nano* **2017,** *11* (1), 526-540.
17. Nelson, B. C.; Petersen, E. J.; Marquis, B. J.; Atha, D. H.; Elliott, J. T.; Cleveland, D.; Watson, S. S.; Tseng, I. H.; Dillon, A.; Theodore, M.; Jackman, J., NIST gold nanoparticle reference materials do not induce oxidative DNA damage. *Nanotoxicology* **2013,** *7* (1), 21-29.
18. Cho, T. J.; MacCuspie, R. I.; Gigault, J.; Gorham, J. M.; Elliott, J. T.; Hackley, V. A., Highly stable positively charged dendron-encapsulated gold nanoparticles. *Langmuir* **2014,** *30* (13), 3883-3893.
19. Reipa, V., NIST Special Publication 1200-12: Reconstitution of 2 nm diameter Silicon Nanoparticles (RM8027) into aqueous solvents. National Institute of Standards and Technology: Gaithersburg, MD, 2015; pp 1-18.
20. Reipa, V.; Purdum, G.; Choi, J., Measurement of nanoparticle concentration using quartz crystal microgravimetry. *J. Phys. Chem. B* **2010,** *114* (49), 16112-16117.
21. ISO, Water quality—Determination of the toxic effect of sediment and soil samples on growth, fertility and reproduction of *Caenorhabditis elegans* (Nematoda). Geneva, Switzerland, 2010; Vol. ISO 10872:2010.
22. Mortimer, M.; Gogos, A.; Bartolome, N.; Kahru, A.; Bucheli, T. D.; Slaveykova, V. I., Potential of hyperspectral imaging microscopy for semi-quantitative analysis of nanoparticle uptake by protozoa. *Environ. Sci. Technol.* **2014,** *48* (15), 8760-7.
23. Badireddy, A. R.; Wiesner, M. R.; Liu, J., Detection, characterization, and abundance of engineered nanoparticles in complex waters by hyperspectral imagery with enhanced darkfield microscopy. *Environ. Sci. Technol.* **2012,** *46* (18), 10081-10088.
24. Schultz, S.; Smith, D. R.; Mock, J. J.; Schultz, D. A., Single-target molecule detection with nonbleaching multicolor optical immunolabels. *Proc. Natl. Acad. Sci. U S A* **2000,** *97* (3), 996-1001.
25. Schindelin, J.; Arganda-Carreras, I.; Frise, E.; Kaynig, V.; Longair, M.; Pietzsch, T.; Preibisch, S.; Rueden, C.; Saalfeld, S.; Schmid, B., Fiji: an open-source platform for biological-image analysis. *Nat. Methods* **2012,** *9* (7), 676-682.
26. Szewczyk, N. J.; Udranszky, I. A.; Kozak, E.; Sunga, J.; Kim, S. K.; Jacobson, L. A.; Conley, C. A., Delayed development and lifespan extension as features of metabolic lifestyle alteration in C. elegans under dietary restriction. *J. Exp. Biol.* **2006,** *209* (20), 4129-4139.
27. Feng, Z. V.; Gunsolus, I. L.; Qiu, T. A.; Hurley, K. R.; Nyberg, L. H.; Frew, H.; Johnson, K. P.; Vartanian, A. M.; Jacob, L. M.; Lohse, S. E.; Torelli, M. D.; Hamers, R. J.; Murphy, C. J.; Haynes, C. L., Impacts of gold nanoparticle charge and ligand type on surface binding and toxicity to Gram-negative and Gram-positive bacteria. *Chem. Sci.* **2015,** *6* (9), 5186-5196.

28. Agashe, H. B.; Dutta, T.; Garg, M.; Jain, N. K., Investigations on the toxicological profile of functionalized fifth-generation poly(propylene imine) dendrimer. *J. Pharm. Pharmacol.* **2006,** *58* (11), 1491-1498.
29. Silva, T.; Pokhrel, L. R.; Dubey, B.; Tolaymat, T. M.; Maier, K. J.; Liu, X., Particle size, surface charge and concentration dependent ecotoxicity of three organo-coated silver nanoparticles: Comparison between general linear model-predicted and observed toxicity. *Sci. Total Environ.* **2014,** *(468–469)*, 968-976.
30. El Badawy, A. M.; Silva, R. G.; Morris, B.; Scheckel, K. G.; Suidan, M. T.; Tolaymat, T. M., Surface charge-dependent toxicity of silver nanoparticles. *Environ. Sci. Technol.* **2011,** *45* (1), 283-287.
31. Shen, M.; Wang, S. H.; Shi, X.; Chen, X.; Huang, Q.; Petersen, E. J.; Pinto, R. A.; Baker, J. R.; Weber, W. J., Polyethyleneimine-mediated functionalization of multiwalled carbon nanotubes: synthesis, characterization, and in vitro toxicity assay. *J. Phys. Chem. C* **2009,** *113* (8), 3150-3156.
32. Schaeublin, N. M.; Braydich-Stolle, L. K.; Schrand, A. M.; Miller, J. M.; Hutchison, J.; Schlager, J. J.; Hussain, S. M., Surface charge of gold nanoparticles mediates mechanism of toxicity. *Nanoscale* **2011,** *3* (2), 410-420.
33. Elimelech, M.; Gregory, J.; Jia, X., Particle Deposition and Aggregation: Measurement, Modelling and Simulation, R.A.F. Williams Ed., Butterworth-Heinemann Ltd.: 2013, 458 pages.
34. Lin, M. Y.; Lindsay, H. M.; Weitz, D. A.; Ball, R. C.; Klein, R.; Meakin, P., Universality in colloid aggregation. *Nature* **1989,** *339* (6223), 360-362.
35. Ungureanu, F.; Halamek, J.; Verdoold, R.; Kooyman, R. P. In *The use of a colour camera for quantitative detection of protein-binding nanoparticles*. In Proceedings of SPIE - The International Society of Optical Engineering. **2009**, (7192), 71920O-1 - 71920O-10.
36. Oldenburg, S. J. Light scattering from gold nanoshells. Rice University Electronic Theses and Dissertations (1999).
37. Treweek, G. P.; Morgan, J. J., The mechanism of E. coli aggregation by polyethyleneimine. *J. Colloid Interface Sci.* **1977,** *60* (2), 258-273.
38. Jiang, W.; Mashayekhi, H.; Xing, B., Bacterial toxicity comparison between nano- and micro-scaled oxide particles. *Environ. Pollut.* **2009,** *157* (5), 1619-25.
39. Ivask, A.; ElBadawy, A.; Kaweeteerawat, C.; Boren, D.; Fischer, H.; Ji, Z.; Chang, C. H.; Liu, R.; Tolaymat, T.; Telesca, D.; Zink, J. I.; Cohen, Y.; Holden, P. A.; Godwin, H. A., Toxicity mechanisms in Escherichia coli vary for silver nanoparticles and differ from ionic silver. *ACS Nano* **2014,** *8* (1), 374-386.
40. Roberts, A. P.; Mount, A. S.; Seda, B.; Souther, J.; Qiao, R.; Lin, S.; Ke, P.; Rao, A. M.; Klaine, S. J., In vivo biomodification of lipid-coated carbon nanotubes by *Daphnia magna*. *Environ. Sci. Technol.* **2007,** *41* (8), 3025-3029.
41. Hunt, P. R.; Olejnik, N.; Sprando, R. L., Toxicity ranking of heavy metals with screening method using adult Caenorhabditis elegans and propidium iodide replicates toxicity ranking in rat. *Food Chem. Toxicol.* **2012,** *50* (9), 3280-90.
42. Ferguson, M.; Boyer, M.; Sprando, R., A method for ranking compounds based on their relative toxicity using neural networking, C. elegans, axenic liquid culture, and the COPAS parameters TOF and EXT. *Open Access Bioinformatics* **2010,** *2010*, 139-144.

43. Sprando, R. L.; Olejnik, N.; Cinar, H. N.; Ferguson, M., A method to rank order water soluble compounds according to their toxicity using Caenorhabditis elegans, a Complex Object Parametric Analyzer and Sorter, and axenic liquid media. *Food Chem. Toxicol.* **2009,** *47* (4), 722-8.
44. Donkin, S. G.; Dusenbery, D. B., A soil toxicity test using the nematode Caenorhabditis elegans and an effective method of recovery. *Arch. Environ. Contam. Toxicol.* **1993,** *25* (2), 145-151.
45. Williams, P. L.; Dusenbery, D. B., Aquatic toxicity testing using the nematode, Caenorhabditis elegans. *Environ. Toxicol. Chem.* **1990,** *9* (10), 1285-1290.
46. Meyer, J. N.; Lord, C. A.; Yang, X. Y.; Turner, E. A.; Badireddy, A. R.; Marinakos, S. M.; Chilkoti, A.; Wiesner, M. R.; Auffan, M., Intracellular uptake and associated toxicity of silver nanoparticles in Caenorhabditis elegans. *Aquat. Toxicol.* **2010,** *100* (2), 140-150.
47. Donkin, S. G.; Williams, P. L., Influence of developmental stage, salts and food presence on various end points using Caenorhabditis elegans for aquatic toxicity testing. *Environ. Toxicol. Chem.* **1995,** *14* (12), 2139-2147.
48. Mao, L.; Liu, C.; Lu, K.; Su, Y.; Gu, C.; Huang, Q.; Petersen, E. J., Exposure of few layer graphene to Limnodrilus hoffmeisteri modifies the graphene and changes its bioaccumulation by other organisms. *Carbon* **2016,** *109*, 566-574.
49. Hanna, S. K.; Cooksey, G. A.; Dong, S.; Nelson, B. C.; Mao, L.; Elliott, J. T.; Petersen, E. J., Feasibility of using a standardized Caenorhabditis elegans toxicity test to assess nanomaterial toxicity. *Environ. Sci. Nano* **2016,** *3* (5), 1080-1089.
50. Rösslein, M.; Elliott, J. T.; Salit, M. L.; Petersen, E. J.; Hirsch, C.; Krug, H. F.; Wick, P., The use of cause-and-effect analysis to design a high quality nano-cytotoxicology assay. *Chem. Res. Toxicol.* **2014,** *27* (10), 1877-1884.
51. Elliott, J. T.; Rosslein, M.; Song, N. W.; Toman, B.; Kinsner-Ovaskainen, A.; Maniratanachote, R.; Salit, M. L.; Petersen, E. J.; Sequeira, F.; Romsos, E. L.; Kim, S. J.; Lee, J.; von Moos, N. R.; Rossi, F.; Hirsch, C.; Krug, H. F.; Suchaoin, W.; Wick, P., Toward achieving harmonization in a nanocytotoxicity assay measurement through an interlaboratory comparison study. *Altex-Altern. Anim. Ex.* **2017,** *34* (2), 201-218.
52. Piret, J. P.; Bondarenko, O. M.; Boyles, M. S. P.; Himly, M.; Ribeiro, A. R.; Benetti, F.; Smal, C.; Lima, B.; Potthoff, A.; Simion, M.; Dumortier, E.; Leite, P. E. C.; Balottin, L. B.; Granjeiro, J. M.; Ivask, A.; Kahru, A.; Radauer-Preiml, I.; Tischler, U.; Duschl, A.; Saout, C.; Anguissola, S.; Haase, A.; Jacobs, A.; Nelissen, I.; Misra, S. K.; Toussaint, O., Pan-European inter-laboratory studies on a panel of in vitro cytotoxicity and pro-inflammation assays for nanoparticles. *Arch. Toxicol.* **2017,** *91* (6), 2315-2330.
53. Kos, M.; Kahru, A.; Drobne, D.; Singh, S.; Kalcikova, G.; Kuhnel, D.; Rohit, R.; Gotvajn, A. Z.; Jemec, A., A case study to optimise and validate the brine shrimp Artemia franciscana immobilisation assay with silver nanoparticles: The role of harmonisation. *Environ. Pollut.* **2016,** *213*, 173-183.
54. Petersen, E. J.; Henry, T. B.; Zhao, J.; MacCuspie, R. I.; Kirschling, T. L.; Dobrovolskaia, M. A.; Hackley, V.; Xing, B.; White, J. C., Identification and Avoidance of Potential Artifacts and Misinterpretations in Nanomaterial Ecotoxicity Measurements. *Environ. Sci. Technol.* **2014,** *48* (8), 4226-4246.

55. Horst, A. M.; Vukanti, R.; Priester, J. H.; Holden, P. A., An assessment of fluorescence- and absorbance-based assays to study metal-oxide nanoparticle ROS production and effects on bacterial membranes. *Small* **2013,** *9* (9-10), 1753-1764.
56. Worle-Knirsch, J. M.; Pulskamp, K.; Krug, H. F., Oops they did it again! Carbon nanotubes hoax scientists in viability assays. *Nano Lett.* **2006,** *6* (6), 1261-1268.

Figure Captions

Figure 1. Toxicity of ENPs to *C. elegans*. A) Impacts of ENPs on growth and B) reproduction using ISO 10872 assay. Nematodes were exposed to ENPs for 96 h with *E. coli* as a food source in half-strength M9. For conditions where no juvenile worms were observed in any of the wells, error bars could not be included because there was 100 % reproduction inhibition for all replicates. C) Impacts of ENPs on growth and D) reproduction in axenic medium. Nematodes were exposed to ENPs for six days in an axenic nutrient medium to avoid interactions with *E. coli*. E) Impacts of ENPs on survival. Nematodes were exposed to ENPs for 24 h in M9 with no food or added nutrients present. Data are presented as mean inhibition of growth ± 1 standard deviation, $n \geq 6$ wells per ENP, each containing 10 adult nematodes for ISO and axenic assays. For the survival assay, n = 3 wells per ENP, each containing five nematodes. Bars with the same letter are not significantly different from one another; Dunn's multiple comparisons test, $p \leq 0.05$.

Figure 2. During the ISO assay, positively charged ENPs produced large agglomerates on the bottom of the wells, and these agglomerates were not seen in wells containing neutral or negatively charged ENPs or in the negative control wells. The same concentrations were used for the different ENPs as were used in Figure 1. These images were taken of wells from the 12-well plates after conducting the ISO assay.

Figure 3. Enhanced darkfield imaging of positively charged Au ENP / *E. coli* agglomeration. A) Representative images of 100 nm bPEI coated Au ENPs incubated with *E. coli* and monitored over time show immediate heteroagglomeration which led to increasingly large agglomerates across the 24 h period. bPEI Au ENPs appear bright yellow and *E. coli* appear faint white. A 10 µm scale bar is in the upper right corner. B) Representative image of control experiment, shown here with 30 nm PEG Au ENP incubated with *E. coli* displays no observable interaction or agglomeration of bacteria with neutral/negative charged particles at any time. Au ENPs appear faint green, *E. coli* appear bright white. A 10 µm scale bar is in the lower right. C) Plot showing small scale agglomeration for bacteria/Au ENP by measuring percentage of particles > 3 $\mu m^2$ in area for each time point and bPEI Au ENP size. Control experiment is 30 nm PEG Au ENP / *E. coli* sample. D) Plot of average agglomerate spatial area measured for each bacteria / bPEI Au ENP size combination and time point. Control comparison is 30 nm PEG Au ENP w/ *E. coli*. For both C) and D) the plotted error bars are ± 1 standard deviation, n = 3 images, and ANOVA with Tukey's *post hoc* analyses for the 24 h data. Bars with the same letter are not significantly different from one another; Tukey's multiple comparisons test, $p \leq 0.05$.

Figure 4. Enhanced darkfield imaging analysis using the ratio of the red (R) and blue (B) channels of a color CCD camera to distinguish between gold nanoparticles and *E. coli* in uniform and mixed solutions. A) Darkfield images of individual solutions of PEG coated Au ENPs (30 nm, 60 nm, and 100 nm in diameter) and *E. coli*. Thirty nm and 60 nm ENPs appear green, 100 nm ENPs appear yellow-orange, and *E. coli* appear white. B) Average R/B ratio for each particle is performed by image analysis and reported as a cumulative distribution plot for the image of PEG coated Au ENPs and *E. coli* bacteria. C) Mie theory calculation of Au ENP scattering as a function of wavelength for 30 nm, 60 nm, and 100 nm sized particles overlaid with the center wavelength for the R and B channels of color camera used for these experiments. D) Table of the R/B ratio values (± 1 standard deviation, n > 500 particles) for Au ENP sizes as calculated by Mie theory and measured for several Au ENP coatings: PEG, PVP, CIT, and bPEI. The measured R/B ratio for *E. coli* is 1.00 ± 0.11. E) Application of using the distinct R/B ratios for Au ENPs and *E. coli* measured in uniform solutions to segment the images of heterogenous combinations of Au ENPs and bacteria. For a representative non-agglomerated mixture: 60 nm PEG coated Au ENPs and *E. coli* shortly after mixing, a reference image is shown alongside a processed image where Au ENPs are colored red at R/B ratio of 1.44 ± 0.32 and bacteria are colored blue at R/B ratio of 1.00 ± 0.11. For a representative agglomerated mixture: 60 nm bPEI coated Au ENPs and *E. coli* after 24 h incubation, a reference image and processed image are shown where the processed image displays agglomerates containing red and blue coloration corresponding to R/B ratios for 60 nm bPEI Au ENPs and *E. coli*.

641 Figure 1

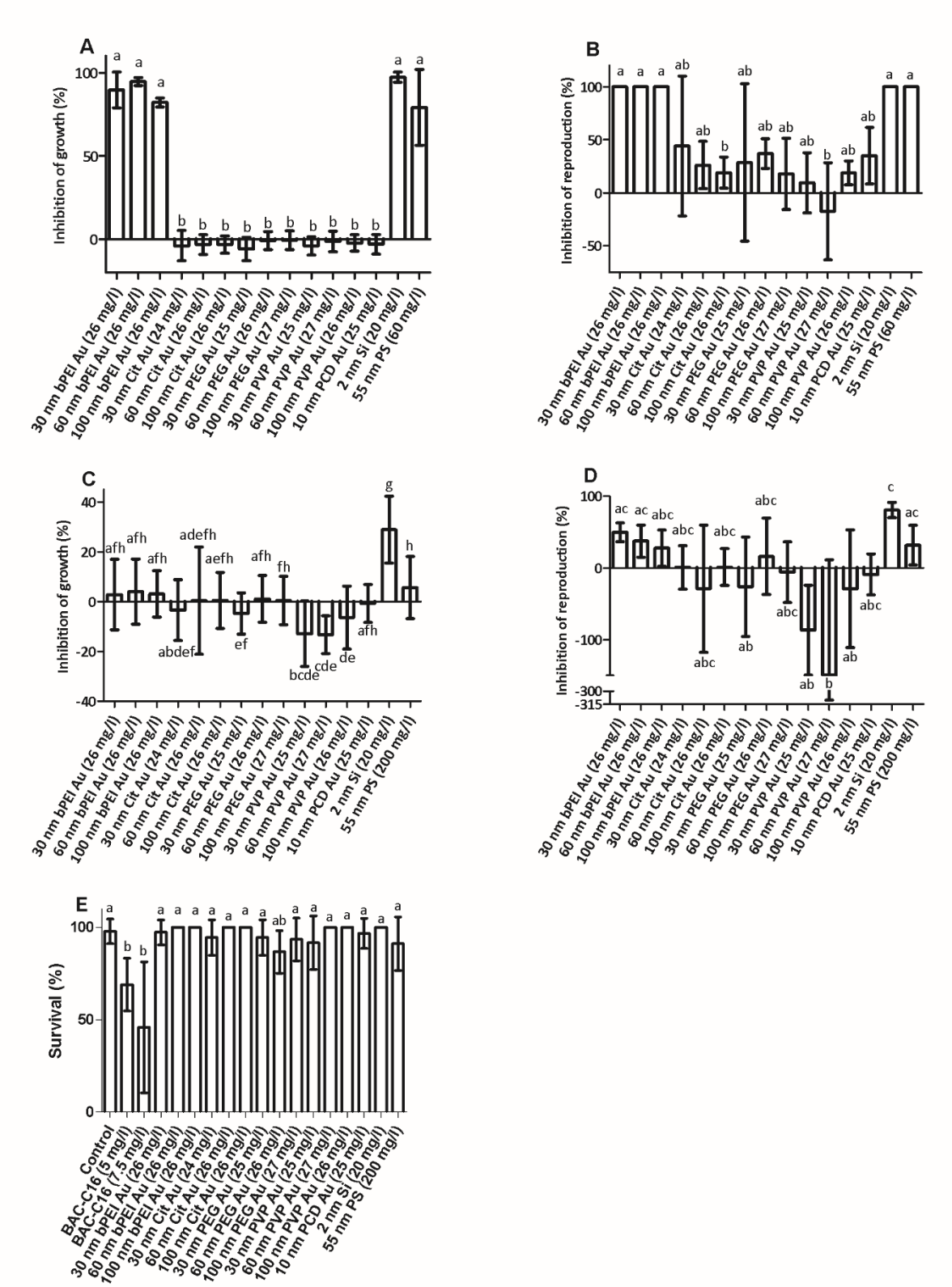


642

643 Figure 2

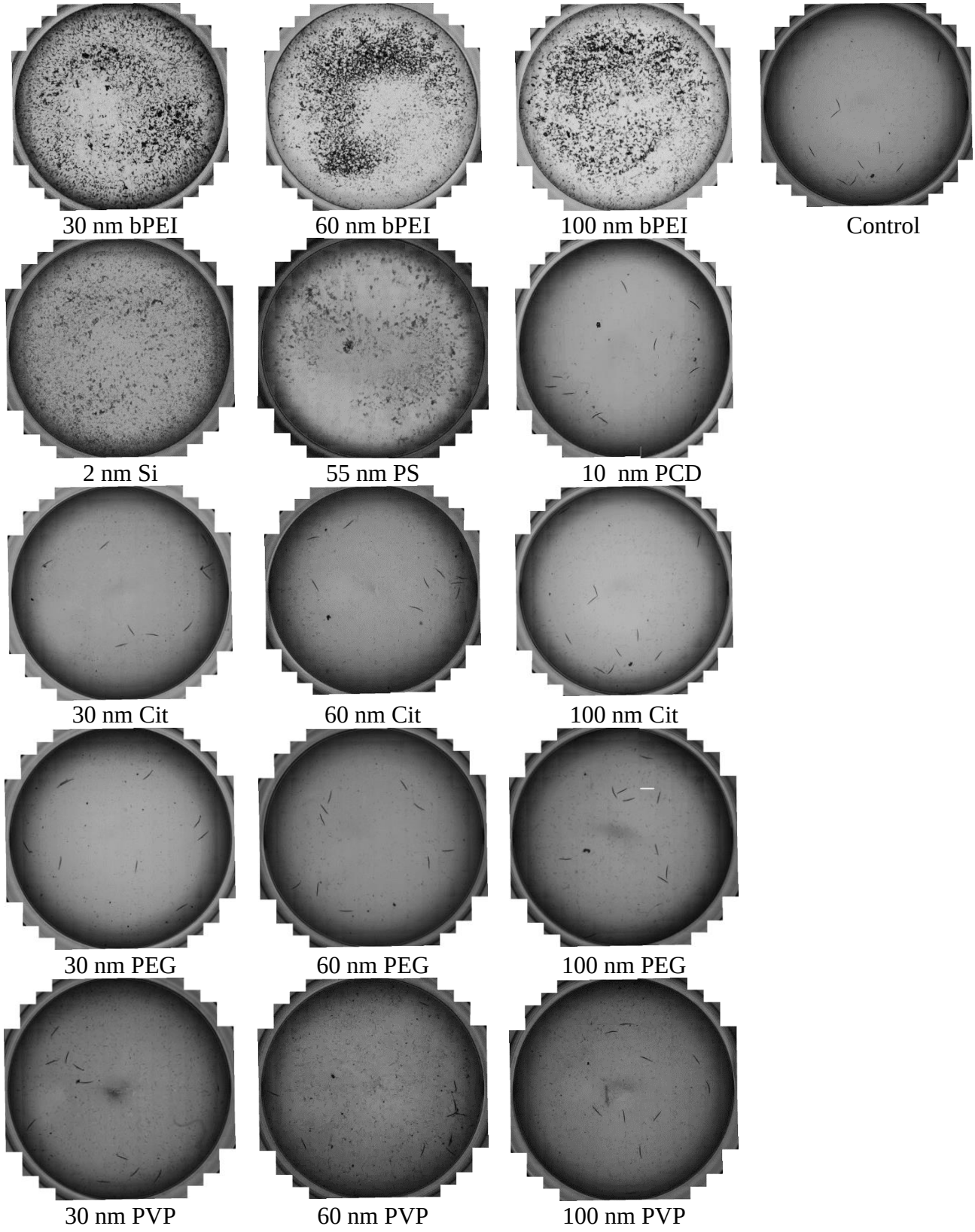
30 nm bPEI
60 nm bPEI
100 nm bPEI
Control
2 nm Si
55 nm PS
10 nm PCD
30 nm Cit
60 nm Cit
100 nm Cit
30 nm PEG
60 nm PEG
100 nm PEG
30 nm PVP
60 nm PVP
100 nm PVP

644 Figure 3

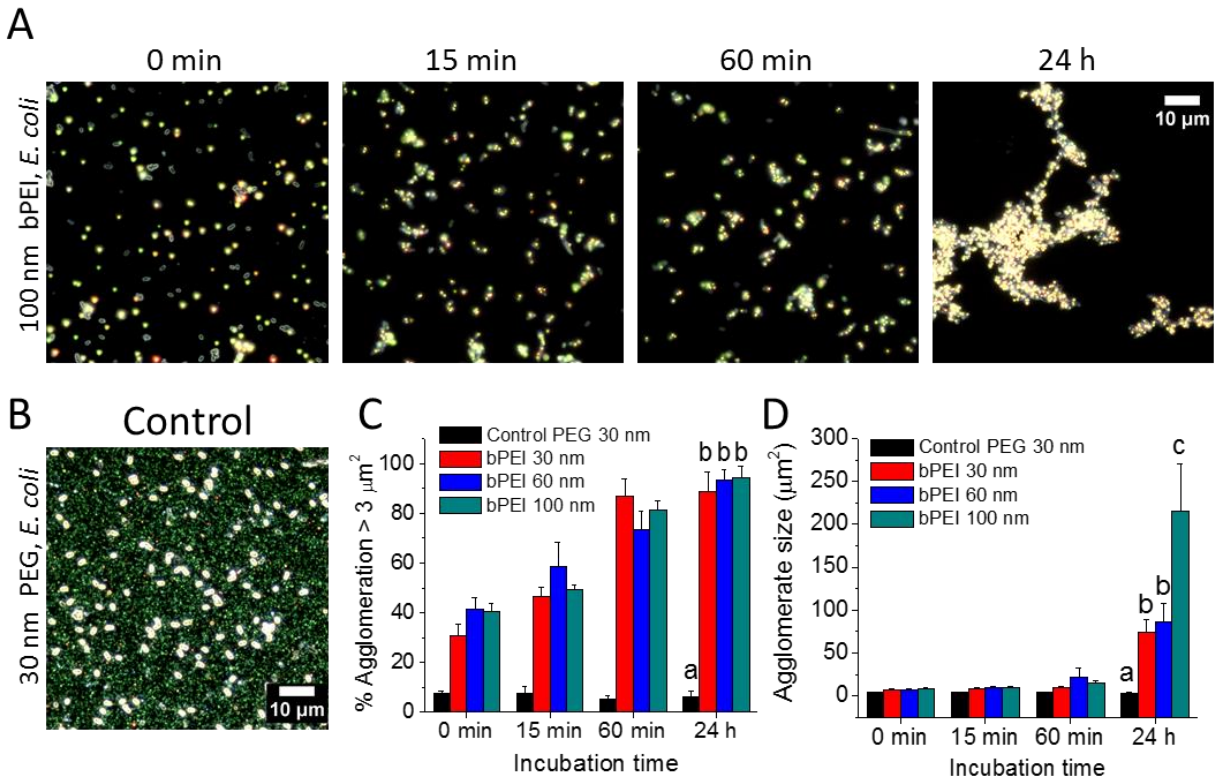


645

646

647

648

649

650 Figure 4

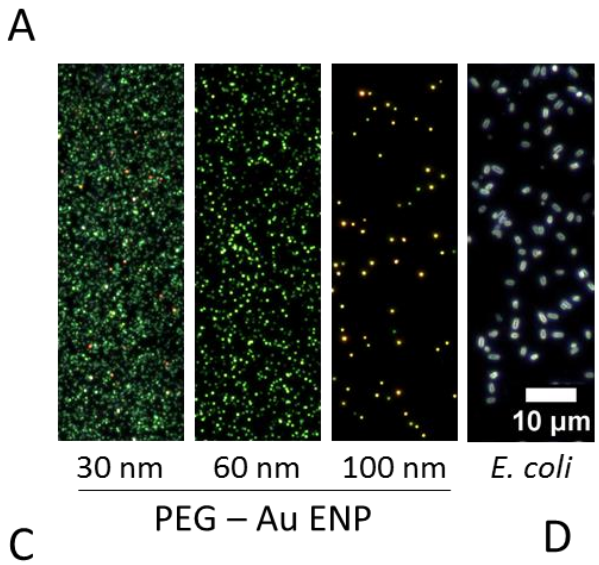


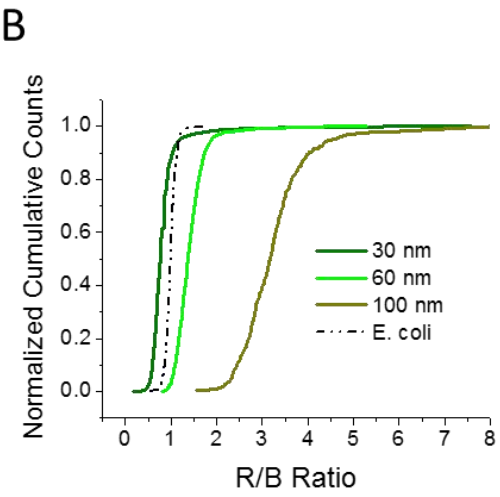


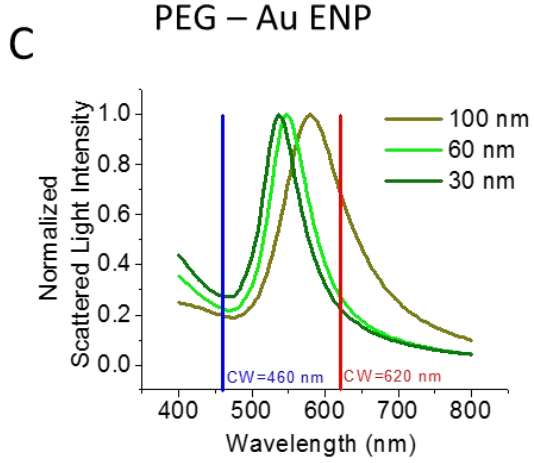


D

| R/B ratio | | | | | |
|---|---|---|---|---|---|
| | Mie theory | PEG | PVP | CIT | bPEI |
| 30 nm | 0.83 | 0.82 ± 0.29 | 0.83 ± 0.17 | 2.63 ± 0.66 | 1.24 ± 0.40 |
| 60 nm | 1.22 | 1.44 ± 0.32 | 1.39 ± 0.24 | 2.76 ± 0.67 | 1.83 ± 0.77 |
| 100 nm | 3.53 | 3.55 ± 0.79 | 3.61 ± 0.84 | 3.09 ± 0.99 | 3.30 ± 0.87 |

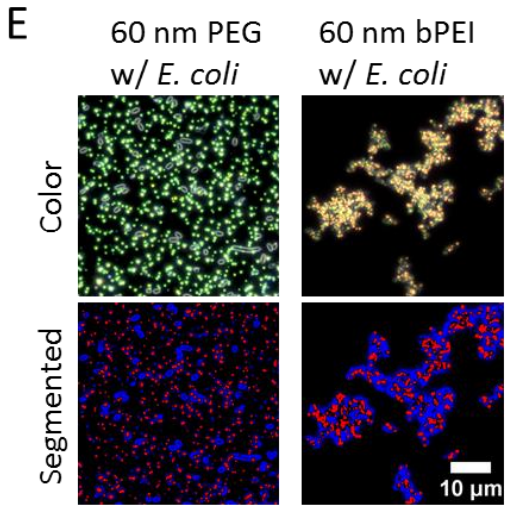


651

652

653